Ashdin Publishing
Journal of Drug and Alcohol Research
Vol. 15 (2026), Article ID 183959, 20 pages
DOI: 10.4303/JDAR/236503

Research Article

In silico Evaluation of Plant-Derived Phytochemicals as Potential Inhibitors of Acetyl-CoA Acyltransferase: A Comparative Study with the Drug Sandoz 58-035 in Lipid Metabolism Disorders

Jharna Maiti[1], Amit Joshi[1*], Shivam Mishra[2]

[1]*Department of Biochemistry, Kalinga University, Atal Nagar-Nava Raipur, India*

[2]*Department of Zoology, S. S. Khanna Girls' Degree College, Prayagraj, India*

[*]*Address Correspondence to Amit Joshi, E-mail: amit.joshi@kalingauniversity.ac.in*

Received: 05 February 2026; Manuscript No: JDAR-26-183959; **Editor assigned:** 09 February 2026; PreQC No: JDAR-26-183959 (PQ); **Reviewed:** 23 February 2026; QC No: JDAR-26-183959; **Revised:** 19 March 2026; Manuscript No: JDAR-26-183959 (R); **Published:** 26 March 2026; DOI: 10.4303/JDAR/236503

Abstract

Lipid metabolic disorders are increasingly recognized as major contributors to cardiovascular diseases, obesity, and related metabolic complications worldwide. Although conventional drugs such as Sandoz-58-035 (CAS 78934-83-5) are widely used to control lipid levels, their long-term administration is often associated with adverse effects, highlighting the need for safer therapeutic alternatives. In the present study, an integrated in silico approach was employed to evaluate plant-derived phytochemicals as potential inhibitors of acetyl-CoA acyltransferase, a key enzyme involved in lipid metabolism. A total of 51 phytochemicals obtained from *Bryophyllum pinnatum*, *Ocimum tenuiflorum*, *Camellia sinensis*, and *Tinospora cordifolia* were screened using molecular docking analysis. Several compounds demonstrated strong binding affinity toward the target enzyme, with binding energies superior to the reference drug, indicating enhanced inhibitory potential. The top-performing phytochemicals were further subjected to pharmacokinetic evaluation using ADME analysis, which revealed favourable absorption, high gastrointestinal availability, and minimal toxicity risks. To validate the stability and dynamic behaviour of the enzyme-phytochemical complexes, molecular dynamics simulations were conducted, confirming stable interactions over the simulation period. Comparative analysis with Sandoz-58-035 drug further supported the effectiveness of selected phytochemicals. Overall, the findings suggest that these natural compounds could serve as promising and safer alternatives for the management of lipid metabolism disorders.

Keywords: Lipid metabolism, Phytochemicals, Molecular docking, ADME analysis, Molecular dynamics simulation, Acetyl-CoA acyltransferase, Sandoz-58-035

Introduction

Lipids represent a broad and diverse group of biomolecules that perform various essential biochemical roles. Their accumulation supports survival by serving as an energy reserve, which can be mobilized and utilized during periods of increased energy demand [1]. As evidenced, abnormal lipid metabolism is associated with many diseases such as type 2 diabetes mellitus, obstructive sleep apnea, coronary artery disease, non-alcoholic fatty liver diseases, cancer, hyperlipidaemia, atherosclerosis, obesity etc. [2]. Abnormal lipid metabolism generally occurs when key enzymes involved in lipid metabolism such as HMG-CoA reductase, lipoprotein lipase, and acyl-CoA acyltransferase (Figure 1) do not function properly [3]. In today's time, lipid metabolic disorder is spreading rapidly across the world. These conditions can be caused by both hereditary and acquired factors. Acquired lipid metabolic disorder often result from multiple causes, with the most basic being diet and lifestyle.

Figure 1: A) HMG CoA reductase, B) Acetyl CoA acetyltransferase, and C) Lipoprotein lipase

Although there are many medications available in the market to manage lipid metabolic disorders such as statin, Sandoz-58-035 etc. but their regular use can lead to several side effects such as muscle pain, liver damage, and gastrointestinal issues [4]. Considering the severe side effects of synthetic drugs, many recent studies have focused on natural products for the treatment of lipid metabolic disorder, among which phytochemicals have gained significant attention. Phytochemicals are naturally occurring compounds found in different parts of plants such as leaves, stems, roots, fruits etc., that are not considered essential nutrients [5]. Several investigations have highlighted the lipid-lowering effects of phytochemicals. These studies are designed to investigate the effects of phytochemicals on acetyl-CoA acetyltransferase, a key enzyme in lipid metabolism. By modulating its activity, phytochemicals may contribute to lowering lipid levels. The outcomes are further compared with standard drug to evaluate their relative efficacy [6].

Materials and Methods

Selection of plants by research literature

With the help of literature review, we selected various four plants species (Figure 2) containing phytochemicals that potentially interfere with lipase enzyme activity. In these studies, we focused those phytochemicals which are present in leaf part of plants. [7].

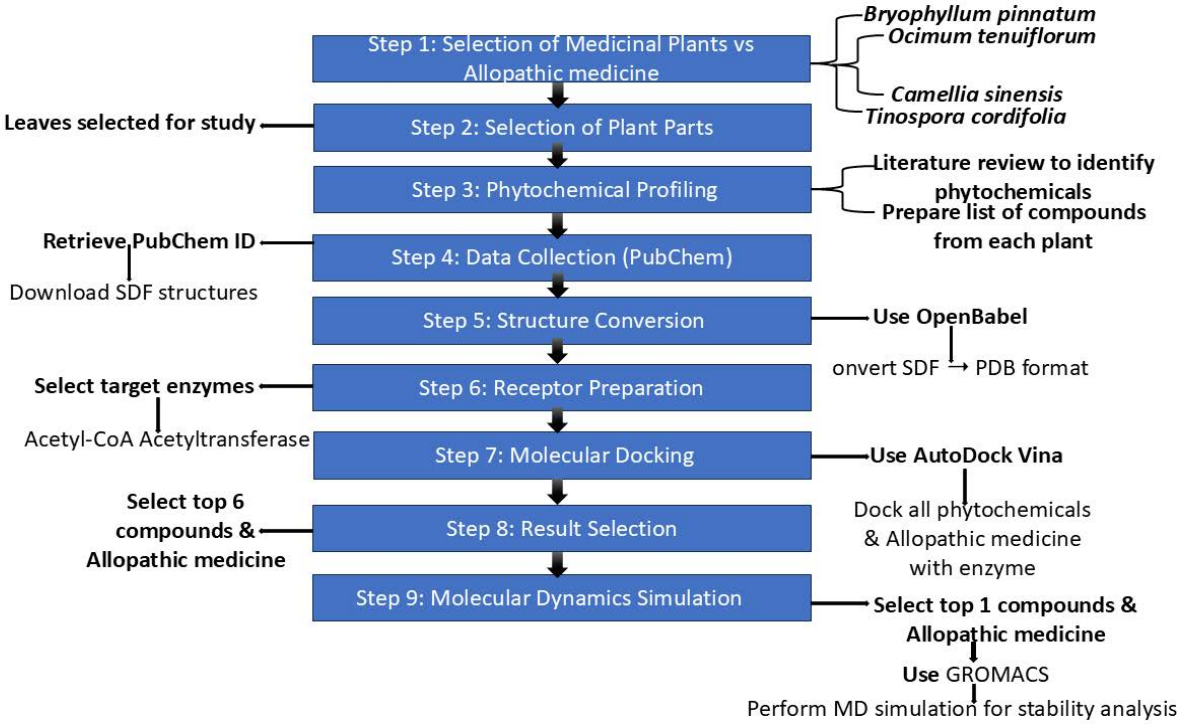

Figure 2: Flow chart of methodology

Retrieval of phytochemicals

The PubChem IDs and SDF formats of all selected phytochemicals were obtained from the NCBI database-[8]. These SDF files were then converted to PDB format using the OpenBabel platform. Babel is an open-source chemical informatics software designed to convert, analyze, and visualize chemical data across a wide range of file formats [9]. This platform built with the PyData Sphinx Theme 0.14.4.

Retrieval of enzyme

The three-dimensional structure (PDB format) of a key enzyme playing a central role in lipid metabolism was retrieved from the RCSB-PDB database [10] and analysed using PyMOL visualization software. PyMOL is a widely used molecular visualization software that allows users to explore and analyze the three-dimensional structures and binding sites [11]. This software maintained and distributed by Schrödinger.

Structural refining

Additional hydrogen atoms, chemical residues, and other structural impurities present in the enzyme (Figure 3) were eliminated using PyMOL software. This step helps prevent any disruption during the docking process [12].

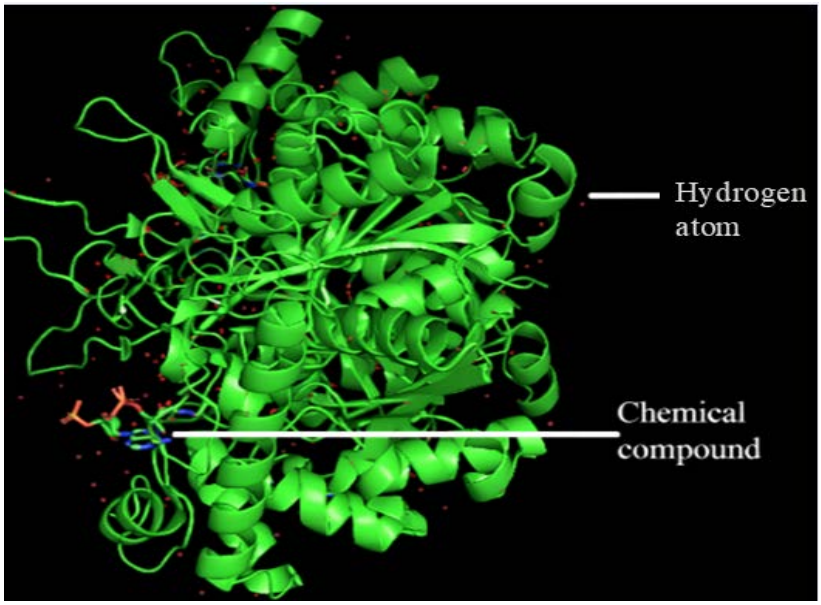

Figure 3: Acyl-CoA Acetyltransferase

Molecular docking analysis

Molecular docking of all phytochemicals with the key enzyme was carried out using AutoDock Vina, based on the PDB structures of both the enzyme and the phytochemicals. AutoDock Vina is an open-source molecular docking tool used to predict how small molecules, such as phytochemicals, interact with a target protein or enzyme [13]. It evaluates various binding poses and ranks them based on a scoring function that estimates the strength and stability of the molecular interaction [14]. Dr. Oleg Trott initially developed and created this tool at the Molecular Graphics Laboratory of the Scripps Research Institute.

ADME analysis

After performing molecular docking, the ADME analysis of the phytochemicals with the target enzymes is carried out using the SwissADME tool [15]. To perform SwissADME analysis, we use the SMILES notation of each phytochemical [16]. ADME analysis involves examining how a substance interacts within the body by evaluating four key processes: Absorption, distribution, metabolism, and excretion [17]. These factors collectively determine the compound's pharmacokinetic profile and its potential as a safe and effective drug. This online platform is managed by the Molecular Modelling Group at the University of Lausanne in collaboration with the SIB Swiss Institute of Bioinformatics.

MD-simulation analysis

Molecular Dynamics (MD) simulation analysis is a computational technique used to study the physical movements of atoms and molecules over time. We performed molecular dynamics simulations of the PDB ID 3SS6 *Bacillus anthracis* acetyl-CoA acetyltransferase in three different systems: the apoprotein (3SS6), the protein in complex with Sandoz-58-035 (3SS6+Sandoz-58-035), and the protein in complex with our proposed phytochemical 21722036 (3SS6+21722036). Molecular dynamics simulations were performed using the GROMACS simulation package [18] with the CHARMM36 force field [19]. Each system was placed in a cubic simulation box with periodic boundary conditions and solvated using the TIP3P water model. To ensure system neutrality, appropriate numbers of sodium and chloride ions were added. Energy minimization was carried out using the steepest descent algorithm until the maximum force converged below 1000 kJ/mol/nm. Following minimization, the systems were equilibrated in two sequential phases: An NVT ensemble for 100 ps at 300 K using the V-rescale thermostat [20], followed by an NPT ensemble for 100 ps at 1 atm pressure using the Parrinello-Rahman barostat. Subsequently, a 100 ns production run was conducted for each system with a time step of 2 fs. Long-range electrostatic interactions were treated using the Particle Mesh Ewald (PME) method, and all covalent bonds involving hydrogen atoms were constrained using the LINCS algorithm. A cutoff distance of 1.2 nm was applied for both van der Waals and short-range electrostatic interactions.Trajectory analyses were performed using built-in GROMACS utilities to evaluate structural stability and dynamic behavior. The Root Mean Square Deviation (RMSD) was calculated to assess conformational stability over the simulation time, while the Root Mean Square Fluctuation (RMSF) was used to evaluate residue-level flexibility. The Radius of gyration (Rg) was computed to examine the compactness of the protein structure, and the Solvent Accessible Surface Area (SASA) was determined to analyze changes in protein surface exposure during the simulation. To further investigate collective motions, Principal Component Analysis (PCA) was performed by constructing and diagonalizing the covariance matrix of atomic positional fluctuations. The eigenvectors corresponding to the largest eigenvalues were used to describe the dominant motions within the system.

Projections along the first two principal components (PC1 and PC2) were used to visualize conformational sampling and dynamic transitions. The Free Energy Landscape (FEL) was constructed based on the projections of PC1 and PC2 to identify stable conformational states. The Gibbs free energy was calculated using the Boltzmann relation, where regions of low free energy correspond to energetically favorable conformations. All graphical representations, including RMSD, RMSF, Rg, SASA, PCA projections, and FEL plots, were generated using OriginPro 2021 software.

Results and Discussion

We selected four plants *Bryophyllum pinnatum*, *Ocimum tenuiflorum*, *Camellia sinensis*, and *Tinospora cordifolia*. These plants collectively contain approximately 51 distinct phytochemicals, the names and PubChem IDs of which are listed in Table 1. The results of the present investigation clearly demonstrate the potential of plant-derived phytochemicals as promising alternatives for the management of lipid metabolism disorders. Several medicinal plants are known for their rich phytochemical content, among which *Bryophyllum pinnatum*, *Ocimum tenuiflorum*, *Camellia sinensis*, and *Tinospora cordifolia* are widely recognized for their therapeutic potential. These plants are notable for containing a diverse range of bioactive compounds with antioxidant, anti-inflammatory, and lipid-lowering properties. *Bryophyllum pinnatum* is rich in flavonoids, terpenoids, and phenolic compounds. *Ocimum tenuiflorum* contains eugenol, ursolic acid, and rosmarinic acid compounds known for their adaptogenic, antimicrobial, and cardioprotective properties. *Camellia sinensis*, is a well-established source of catechins like Epigallocatechin Gallate (EGCG), which has been extensively studied for its antioxidant and lipid-lowering effects. *Tinospora cordifolia*, another widely used herb in traditional medicine, offers alkaloids, diterpenoids, and glycosides with immunomodulatory and hepatoprotective effects. When compared to other phytochemical-rich plants such as *Curcuma longa*, *Withania somnifera*, or *Azadirachta indica*, the above four plants hold unique advantages. For instance, *Curcuma longa* is potent anti-inflammatory agent, while *Withania somnifera* contains with anolides that help manage stress and hormonal balance. *Azadirachta indica* offers strong antibacterial and antiparasitic compounds like nimbin and azadirachtin but not good modulator of lipid metabolic disorder. While many medicinal plants possess valuable phytochemicals, *Bryophyllum pinnatum*, O*cimum tenuiflorum*, *Camellia sinensis*, and *Tinospora cordifolia* stand out for their well-documented pharmacological actions and balanced combination of bioactive compounds, especially in the context of antioxidant defence, metabolic regulation, and immune support. Lipid-lowering drugs, particularly Sandoz-58-035, are widely prescribed for the management of hypercholesterolemia and the prevention of cardiovascular diseases. Sandoz-58-035 work by inhibiting Acetyl-CoA acyltransferase, a key enzyme in the fatty acid breakdown and synthesis of acetyl CoA, thereby reducing acetyl CoA levels in the blood. Despite their efficacy, long-term Sandoz-58-035 use has been associated with several adverse effects. According to meta-analyses by Reith et al. and Yuhua Jiang. Long term use of statins and other synthetic medications is frequently associated with a range of adverse effects, including muscle pain, liver damage, and gastrointestinal disturbances, myalgia, elevated liver enzyme levels, and other serious side effects. In contrast, the plant derived phytochemicals we have utilized are not linked to such side effects, making them a safer and more favourable option for long term therapy like Catechins from *Camellia sinensis* have been shown to reduce total cholesterol and LDL levels through inhibition of cholesterol absorption and modulation of hepatic lipid metabolism. Kaempferol is a naturally occurring flavonoid found in *Bryophyllum pinnatum* has drawn significant scientific attention for its therapeutic potential in managing lipid metabolic disorders, including hyperlipidemia, obesity, Non-Alcoholic Fatty Liver Disease (NAFLD), and atherosclerosis. Berberine, found in *Tinospora cordifolia*, activates AMP-activated protein kinase, leading to improved lipid and glucose metabolism.

Table 1: Phytochemicals name, sources, and PubChem ID

S. no.	Plants	S. no.	Phytochemical name	PubChem CID
1	*Bryophyllum pinnatum*	1	Syringic acid	10742
		2	4-hydroxy-3-methoxy-cinnamic acid	709
		3	P-hydroxycinnamic acid	637542
		4	Para coumaric acid	1549106
		5	Protocatechuic acid	528594
		6	Phosphoenolpyruvate	1005
		7	Astragalin	5282102
		8	3,8-dimethoxy-4,5,7-trihydroxyflavone	131752831
		9	Friedelin	91472
		10	Epigallocatechin-3-o-syringate	65064
		11	Luteolin	67110957
		12	Rutin	16218542
		13	Kaempferol	5280863

		14	Quercetin	5280343
		15	Quercetin 3L-rhamonsido-L-arabino furanoside	5488539
		16	Quercetin-3-O diarabinoside	12309865
		17	Kaempferol-3-glucoside	44258798
		18	Kaempferol-3-O-α-L-arabinopyranosyl	57401109
		19	α-L-rhamno pyranoside	10698716
		20	Quercetin-3-O-α-L-arabino pyranosyl	21722036
		21	α-L-rhamno pyranoside	44259288
2	*Ocimum tenuiflorum*	1	Caffeic acid	689043
		2	Chlorogenic acid	1794427
		3	Vanillic acid	8468
		4	Vanillin	71309238
		5	Isothymusin	630253
		6	Cirsimartin	188323
		7	Orientin	5281675
		8	Isoorientin	114776
		9	Isovitexin	162350
		10	Sesquiterpenoids	139087999
		11	Abietane diterpenoid	6857485
		12	Oleane triterpenoids	9548717
		13	Ursane triterpenoids	9548870
3	*Camellia sinensis*	1	Gallocatechin	65084
		2	Flavan-3-ols	3707243
		3	Epicatechin	72276
		4	Epigallocatechin	72277
		5	Epicatechin gallate	65056
		6	5-caffeoylquinic acid	5315832
		7	Theogallin	442988
4	*Tinospora cordifolia*	1	Tembetarine	167718
		2	Choline	305
		3	Magnoflorine	73337
		4	Berberine	2353
		5	Tinosporin	42607646
		6	Isocolumbin	226036
		7	Palmetine	19009
		8	Jatrorrhizine	72323
		9	Aporphine	114911
		10	Tetrahydropalmatine	72301

The three-dimensional crystal structure of *Bacillus anthracis* acetyl CoA acetyltransferase was obtained from the RCSB Protein Data Bank (PDB) (Figure 1 B). Structural preprocessing was performed using PyMOL, during which all heteroatoms, including co-crystallized ligands, solvent molecules, and non-essential hydrogen bonds, were systematically removed to prepare the protein for subsequent molecular docking studies (Figure 4).

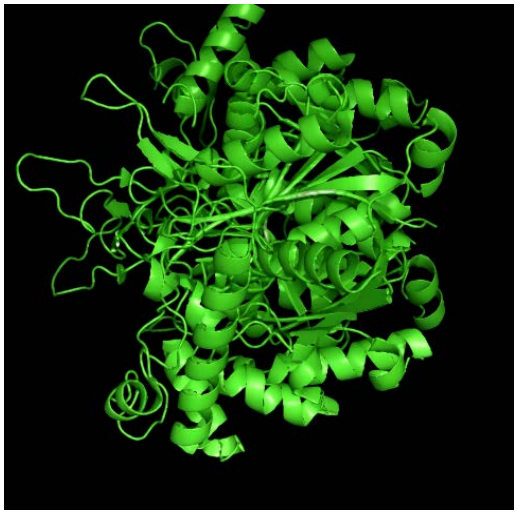

Figure 4: Removed bound chemical ligands and hydrogen atom from Acyl-CoA Acetyltransferase

Molecular docking analysis

Using AutoDock Vina, molecular docking was performed between acetyl CoA acyltransferase phytochemicals present in all four selected plants and drug Sandoz-58-035 responsible for inhibition of acetyl CoA acyltransferase. In this analysis, enzyme was considered as a receptor, while all phytochemicals and drug were treated as ligands. Enzyme-phytochemical complexes exhibiting binding energies greater than -8.5 kcal/mol and enzyme-Sandoz-58-035 complexes exhibiting binding energies greater than -7 were shown here (Table 2). We selected seven enzyme-phytochemical docking complexes and enzyme-drug docking complex that showed good docking results and studied their bond interactions and participating amino acids using Protein Phytochemical Interaction Profiler (PLIP) software and Discovery Studio. Molecular docking studies of Acetyl-CoA Acyltransferase (ACOAT) with different phytochemicals revealed a variety of molecular interactions. When ACOAT was docked with rutin (PubChem ID: 5280805), hydrogen bonds were observed with glutamine and valine residues. In addition, phenylalanine was involved in both hydrophobic interactions and π stacking with the rutin molecule. Phenylalanine at position 29A participates in a π-stacking bond with the ligand. The distance between the aromatic ring of phenylalanine and the phytochemical is 4.05 Å. The angle of interaction is 20.08, The offset is 1.42 Å, further confirming the stability of the parallel alignment. The phytochemical atoms involved in this interaction are 1, 2, 3. Docking of the same enzyme with another phytochemical Quercetin 3L-rhamonsido-L-arabino furanoside (5488539) showed hydrophobic interactions with phenylalanine, glutamine, and aspartic acid. Hydrogen bonds were formed with tyrosine, arginine, serine, glutamine, aspartic acid, and histidine. π-stacking was seen with phenylalanine and histidine, and a salt bridge interaction was observed with arginine. In the π-stacking section, three interactions are observed. The first interaction involves phenylalanine 29 A, forming a π-stacking bond with the ligand. The measured distance is 4.5 Å, the angle of interaction is 27.25 degrees, and the offset is 1.82 Å. This interaction is categorized as a parallel stacking type. The phytochemicalatoms involved in this interaction include 1, 2, 3, 4, 5, 21. The next two π-stacking interactions involve histidine at 144 A with a distance of 5.23 Å, angle 88.79 degrees, and offset 1.83 Å. The third interaction shows histidine interacting at a distance of 5.29 Å, with angle 87.31 degrees and offset 1.88 Å. The phytochemicalatoms involved in these histidine interactions are 1, 2, 3, 4, 5, 21 for the second interaction, and 4, 5, 6, 7, 8,9 for the third. In the salt bridge interaction section, one interaction is noted between arginine at 80A. The distance is 5.29 Å. Specific phytochemicalatoms participated in this interaction are 24 and 23. When ACOAT was docked with 3,8-dimethoxy-4,5,7-trihydroxyflavone (131752831), hydrophobic interactions involved phenylalanine, glutamine, and aspartic acid, while hydrogen bonds were shown with tyrosine, arginine, serine, phenylalanine, and histidine, and a salt bridge was again formed with 80A arginine, distance was 4.8 Å, phytochemicalatom 27 and 26 carboxylate was involved. The π-stacking was seen with 144A histidine and the distance, angle offset and stacking type was 5.04, 78.7, 0.82, T shaped seen. The phytochemical atom 2, 4, 7, 8, 9, 24 involved. In the case of syringic acid (10742), phenylalanine participated in hydrophobic interactions, whereas hydrogen bonding involved tyrosine, arginine, histidine, and glutamine, with a salt bridge identified for arginine and distance was 3.74 Å, protein positive and phytochemical atom 10 and 11 carboxylate was involved. Docking of ACOAT with Kaempferol-3-O-α-L-arabinopyranosyl (57401109) resulted in hydrophobic interactions involving valine and arginine residues, glycine, glutamic acid, and histidine. Both arginine and histidine were involved in and salt bridge formation. The distance with arginine and histidine was 4.97 Å and 5.32 Å, both shown protein positive, for arginine phytochemical atom 30 and 29 carboxylate and for histidine phytochemical atom 37 and 36 was involved. Carboxylate ACOAT dock with Quercetin-3-O-α-L-arabino pyranosyl (21722036) on that case glutamine, serine, arginine was formed hydrogen bond, phenylalanine, tyrosine and valine are involved in hydrophobic interactions, π-stacking was seen with phenylalanine, where the distance 4.36 Å, angle 28.81 degree, offset 1.27, stacking type: Parallel and 21, 22, 23, 24, 25, 26 phytochemicalatom involved and salt bridge was seen with histidine where the distance 5,2 protein was positive, 30 and 29 phytochemicalatom carboxylate

was involved seen. ACOAT with α-L-rhamno pyranoside (10698716) phenylalanine, leucine, valine, aspartic acid and glutamine was involved in hydrophobic interaction, arginine serine, glutamine, tyrosine and aspartate were formed hydrogen bond phenylalanine involved π-stacking and 80A arginine was involved salt bridge the distance of salt bridge was 4.22 Å and 5 seen and carboxylate group of phytochemical was involved. one carboxylate presents in 35 and 28 position another was 39 and 38. The distance, angle offset and stacking type of π-stacking was seen 4.29,16.53,1.71 and P where 1,2 and 3 phytochemical atom was involved (Figures 5 to 12 and Tables 3 to 10). Additionally, the bond types and bond lengths within the enzyme-phytochemical complex were analysed using discovery studio for a detailed structural characterization.

Table 2: Molecular docking enzyme with phytochemicals and binding energy

S. no	Enzyme	Drug and phytochemical (Pubchem Chemical ID)	Binding score/Binding energy (Kcal/mol)
1	Acyl-CoA Acyltransferase	Sandoz (147031)-drug	-7.6
		Rutin (5280805)	-9.7
		Quercetin 3L-rhamonsido-L-arabino furanoside (5488539)	-9.5
		Quercetin-3-O diarabinoside (12309865)	-9.3
		Quercetin-3-O-α-L-arabino pyranosyl (21722036)	-10
		Kaempferol-3-glucoside (44258798)	-9.3
		Kaempferol-3-O α-L-arabinopyranosyl (57401109)	-10
		α-L-rhamno pyranoside (10698716)	-10
		3,8-dimethoxy-4,5,7 trihydroxyflavone (131752831)	-9.5
		Epigallocatechin-3-o-syringate (65064)	-10.7
		Syringic acid (10742)	-9.5
		Isovitexin (162350)	-9.1
		Orientin (5281675)	-9.2
		Epicatechin gallate (65056)	-9.4
		Quercetin (5280343)	-8.8
		Luteolin (5280445.957)	-8.6

Table 3: Bonds interaction for molecular interaction between ACOAT with Rutin (5280805)

Hydrophobic interactions									
S. no.	**Residue**	**AA**	**Distance**	**Phytochemical A**	**Protein atom**				
1	29A	PHE	3.69	8	298				
Hydrogen bonds									
S. no.	**Residue**	**AA**	**Distance H-A**	**Distance D-A**	**Donor angle**	**Protein donor**	**Side chain**	**Donor atom**	**Acceptor atom**
1	33A	GLN	3.05	3.61	117.48	X	✓	11	337
2	81A	VAL	2.02	2.98	155.96	✓	X	803	12 [O3]
3	81A	VAL	3.19	4.08	153.48	X	X	12 [O3]	806

Table 4: Bonds interaction for molecular interaction between ACOAT with Quercetin 3L-rhamonsido-L-arabino furanoside (5488539)

Hydrophobic interactions									
Index	**Residue**	**AA**	**Distance**	**Phytochemical atom**					
1	29A	PHE	3.62	16	324				
2	118A	GLN	3.77	20	1177				
3	140A	ASP	3.69	8	1397				
Hydrogen bonds									
Index	**Residue**	**AA**	**Distance H-A**	**Distance D-A**	**Donor angle**	**Protein donor**	**Side chain**	**Donor atom**	**Acceptor atom**
1	37A	TYR	3.64	3.95	101.58	✓	✓	403 [O3]	22 [O2]
2	65A	ARG	2.31	3.17	141.09	✓	✓	674 [Ng+]	25 [O3]
3	80A	ARG	1.79	2.81	171.42	✓	X	810 [Nam]	24 [O3]

4	80A	ARG	2.49	3.11	118.65	✓	✓	820 [Ng+]	25 [O3]
5	116A	SER	2.14	2.86	128.75	X	X	27 [O3]	1161 [O2]
6	116A	SER	3.13	3.76	124.82	✓	✓	1163 [O3]	26 [O3]
7	118A	GLN	2.23	3.15	149.42	✓	X	1172 [Nam]	29 [O3]
8	125A	TYR	2.28	2.71	105.52	X	✓	28 [O3]	1255 [O3]
9	125A	TYR	2.36	3.3	164.29	X	✓	29 [O3]	1255 [O3]
10	140A	ASP	2.16	3.06	163.17	✓	✓	1399 [O3]	31 [O3]
11	140A	ASP	2.67	3.06	104.55	X	✓	31 [O3]	1399 [O3]
12	144A	HIS	2.8	3.3	110.28	✓	□	1436 [Npl]	27 [O3]

Table 5: Bonds interaction for molecular interaction between ACOAT with 3,8-dimethoxy-4,5,7 trihydroxyflavone (131752831)

Hydrophobic interactions									
Index	**Residue**	**AA**	**Distance**	**Phytochemical atom**	**Protein atom**				
1	37A	TYR	3.59	5	404				
2	81A	VAL	3.47	19	834				
3	118A	GLN	3.99	22	1180				
Hydrogen bonds									
Index	**Residue**	**AA**	**Distance H-A**	**Distance D-A**	**Donor angle**	**Protein donor**	**Side chain**	**Donor atom**	**Acceptor atom**
1	37A	TYR	3.37	3.97	122.6	✓	✓	406 [O3]	32 [O3]
2	65A	ARG	2.91	3.69	134.3	✓	✓	677 [Ng+]	31 [O3]
3	78A	ILE	2.14	3.05	154	X	X	29 [O3]	802 [O2]
4	80A	ARG	2.23	3.2	157.6	✓	X	813 [Nam]	27 [O3]
5	80A	ARG	2.15	2.89	128.3	✓	✓	823 [Ng+]	31 [O3]
6	80A	ARG	3.63	3.96	101.5	✓	✓	822 [Ng+]	32 [O3]
7	116A	SER	1.96	2.87	147.3	✓	X	1161 [Nam]	29 [O3]
8	125A	TYR	2.59	2.95	102.7	✓	✓	1258 [O3]	33 [O3]
9	125A	TYR	2.42	2.95	114.2	X	✓	33 [O3]	1258 [O3]

Table 6: Bonds interaction for molecular interaction between ACOAT with Syringic acid (10742)

Hydrophobic interactions									
Index	**Residue**	**AA**	**Distance**	**Phytochemical atom**	**Protein atom**				
1	29A	PHE	3.57	6	300				
2	29A	PHE	3.66	3	302				
Hydrogen bonds									
Index	**Residue**	**AA**	**Distance H-A**	**Distance D-A**	**Donor angle**	**Protein donor**	**Side chain**	**Donor atom**	**Acceptor atom**
1	37A	TYR	2.27	2.71	107.35	✓	✓	381 [O3]	11 [O.co2]
2	37A	TYR	2.29	2.71	105.17	X	✓	11 [O.co2]	381 [O3]
3	80A	ARG	2.48	3.24	130.23	✓	X	788 [Nam]	10 [O.co2]
4	118A	GLN	2.18	3.05	142.76	✓	✓	1157 [Nam]	13 [O3]
5	144A	HIS	2.11	3.05	152.48	✓	✓	1414 [Npl]	13 [O3]

Table 7: Bonds interaction for molecular interaction between ACOAT with Kaempferol-3-O α-L-arabinopyranosyl (57401109)

Hydrophobic interactions									
Index	**Residue**	**AA**	**Distance**	**Phytochemical atom**	**Protein atom**				
1	81A	VAL	3.73	21	841				
2	81A	VAL	3.69	20	843				
3	88A	ARG	3.77	13	894				
Hydrogen bonds									
Index	**Residue**	**AA**	**Distance H-A**	**Distance D-A**	**Donor angle**	**Protein donor**	**Side chain**	**Donor atom**	**Acceptor atom**
1	33A	GLN	2.25	3.18	150.78	✓	✓	370 [Nam]	28 [O2]
2	83A	SER	2.9	3.63	134.63	✓	✓	858 [O3]	31 [O3]
3	83A	SER	2.37	3.11	129.05	✓	X	853 [Nam]	33 [O3]
4	88A	ARG	2.99	3.43	107.44	✓	✓	896 [Ng+]	33 [O3]
5	88A	ARG	3.19	3.6	105.67	✓	✓	899 [Ng+]	33 [O3]
6	93A	GLY	2.83	3.3	108.75	✓	X	937 [Nam]	31 [O3]
7	116A	SER	3.14	3.89	131.81	✓	X	1168 [Nam]	35 [O3]
8	116A	SER	3.34	3.9	118.34	X	X	35 [O3]	1171 [O2]
9	118A	GLN	2.44	3.28	139.16	✓	✓	1189 [Nam]	40 [O3]
10	139A	GLU	2.53	3.01	110.21	X	✓	39 [O3]	1400 [O.co2]
11	144A	HIS	3.06	3.78	128.35	✓	✓	1446 [Npl]	40 [O3]

Table 8: Bonds interaction for molecular interaction between ACOAT with Quercetin-3-O-α-L-arabino pyranosyl (21722036)

Hydrophobic interactions									
Index	**Residue**	**AA**	**Distance**	**Phytochemical atom**	**Protein atom**				
1	29A	PHE	3.49	23	331				
2	37A	TYR	3.71	23	412				
3	81A	VAL	3.92	18	844				
Hydrogen bonds									
Index	**Residue**	**AA**	**Distance H-A**	**Distance D-A**	**Donor angle**	**Protein donor**	**Side chain**	**Donor atom**	**Acceptor atom**
1	33A	GLN	2.62	3.16	113	✓	✓	372 [Nam]	37 [O3]
2	80A	ARG	2.96	3.61	122.2	✓	X	822 [Nam]	28 [O2]
3	83A	SER	2.69	3.23	112.9	✓	X	855 [Nam]	35 [O3]
4	83A	SER	2.96	3.52	117.7	X	✓	35 [O3]	860 [O3]
5	116A	SER	2.31	3.23	153.8	X	X	31 [O3]	1173 [O2]
6	116A	SER	2.42	3.41	163.1	✓	X	1170 [Nam]	40 [O3]
7	116A	SER	3.13	3.62	112.5	X	X	40 [O3]	1173 [O2]
8	118A	GLN	3.08	3.69	119.1	✓	✓	1191 [Nam]	39 [O3]

Table 9: Bonds interaction for molecular interaction between ACOAT α-L-rhamno pyranoside (10698716)

Hydrophobic interactions					
Index	**Residue**	**AA**	**Distance**	**Phytochemical atom**	**Protein atom**
1	29A	PHE	3.71	11	338
2	43A	LEU	3.98	25	469
3	81A	VAL	3.41	12	844
4	118A	GLN	4	15	1190
5	140A	ASP	3.68	6	1410

Hydrogen bonds									
Index	**Residue**	**AA**	**Distance H-A**	**Distance D-A**	**Donor angle**	**Protein donor**	**Side chain**	**Donor atom**	**Acceptor atom**
1	80A	ARG	2.31	3.26	153.83	✓		823 [Nam]	35 [O3]
2	116A	SER	2.62	3.48	141.82	✓	X	1171 [Nam]	36 [O3]
3	116A	SER	2.38	2.96	117.75	X	X	36 [O3]	1174 [O2]
4	116A	SER	2.21	3.02	139.22	X	X	37 [O3]	1174 [O2]
5	118A	GLN	2.28	3.03	129.77	✓	X	1185 [Nam]	34 [O3]
6	125A	TYR	3.18	3.98	140.87	X	✓	34 [O3]	1268 [O3]
7	140A	ASP	2.13	3.06	169.96	✓	✓	1412 [O3]	32 [O3]
8	140A	ASP	2.49	3.06	118	X	✓	32 [O3]	1412 [O3]

Table 10: Bonds interaction for molecular interaction between ACOAT and Sandoz (147031)

Hydrophobic interactions					
Index	**Residue**	**AA**	**Distance**	**Phytochemical atom**	**Protein atom**
1	29B	PHE	3.52	10	1460
2	29B	PHE	3.66	18	1458
3	37B	TYR	3.63	20	1525
4	81B	VAL	3.56	13	1876
5	118B		3.97	23	2152
6	142B	ILE	3.92	23	2352

Hydrogen bonds									
Index	**Residue**	**AA**	**Distance H-A**	**Distance D-A**	**Donor angle**	**Protein donor**	**Side chain**	**Donor atom**	**Acceptor atom**
1	37B	TYR	3.44	3.96	117.35	✓	✓	1527 [O3]	3 [N3]
2	80B	ARG	2	2.85	142.67	✓	X	1861 [Nam]	25 [O2]
3	80B	ARG	2.23	3.14	151.96	✓	✓	1871 [Ng+]	25 [O2]

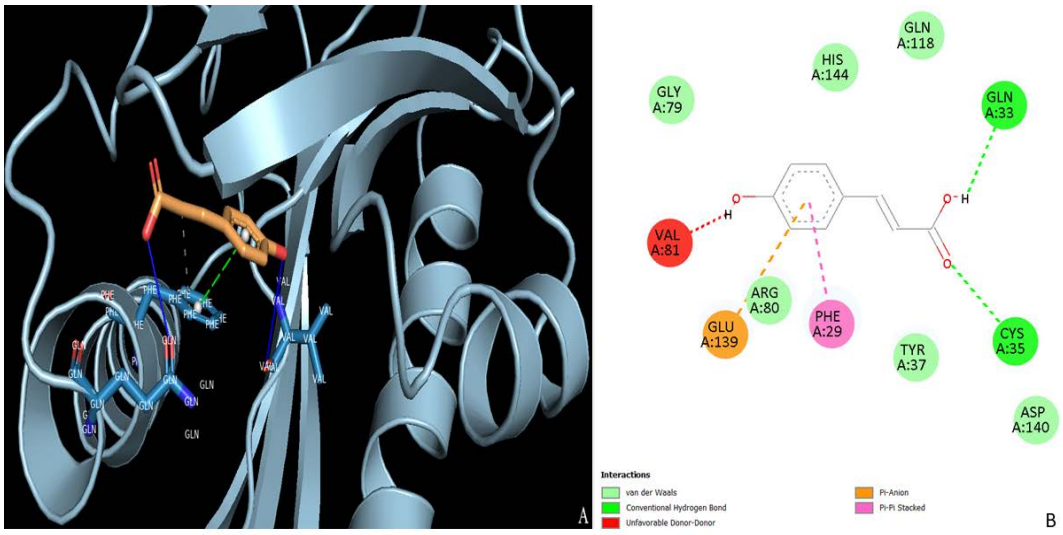

Figure 5: Molecular interaction between ACOAT with Rutin (5280805)

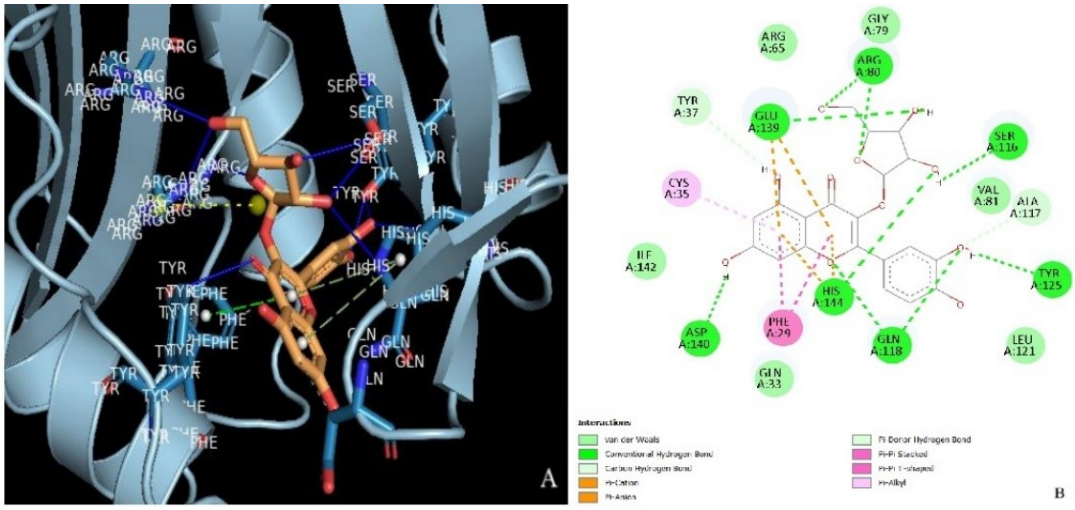

Figure 6: Molecular interaction between ACOAT with Quercetin 3L-rhamonsido-L-arabino furanoside (5488539)

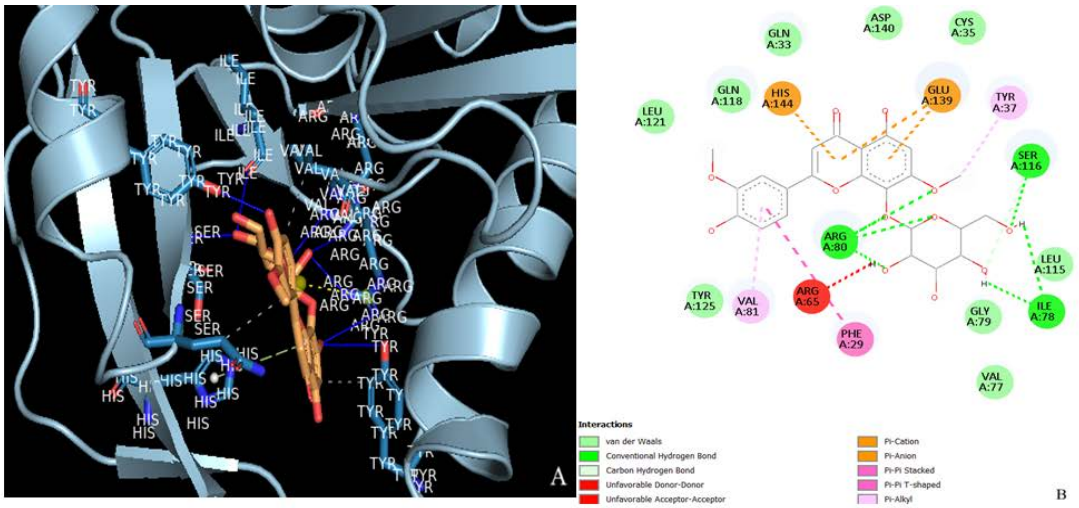

Figure 7: Molecular interaction between ACOAT with 3,8-dimethoxy-4,5,7-trihydroxyflavone (131752831)

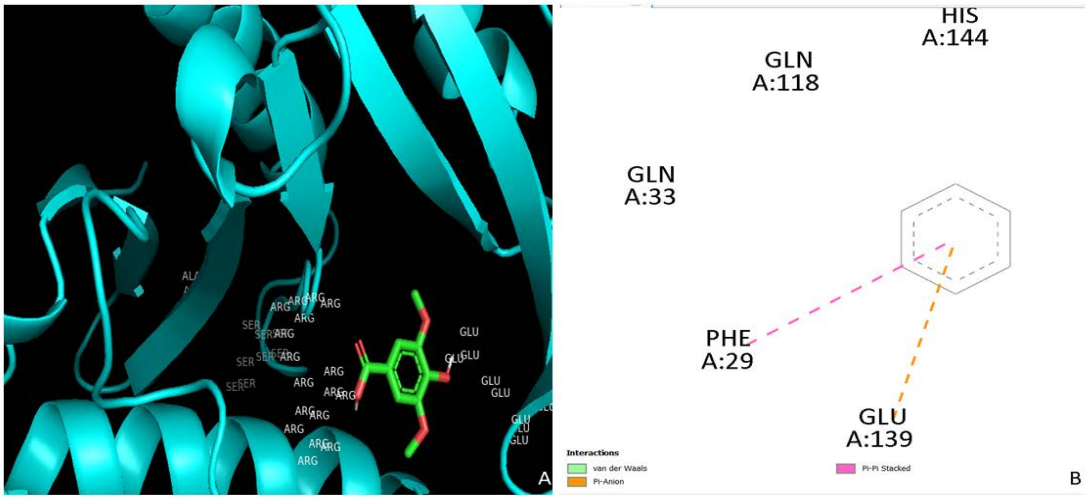

Figure 8: Molecular interaction between ACOAT with Syringic acid (10742)

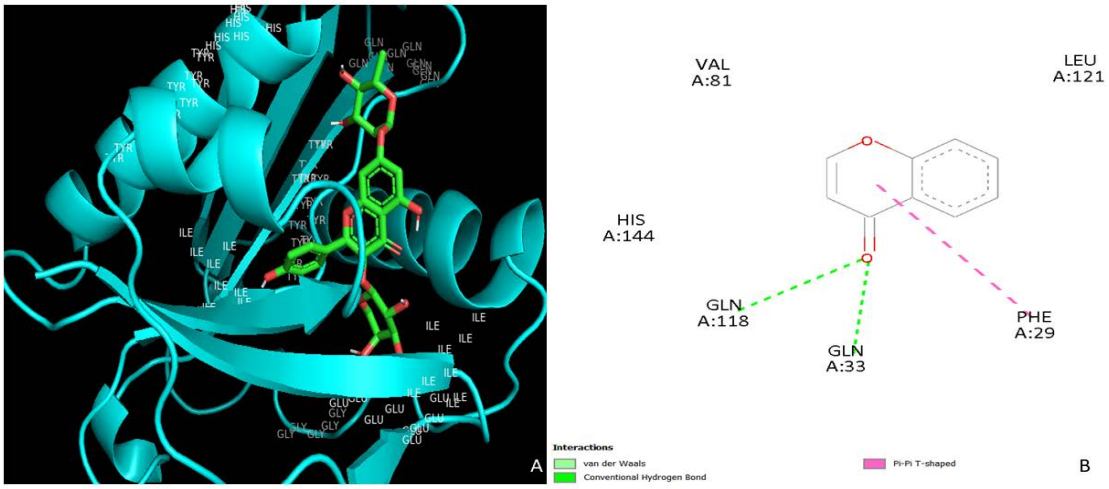

Figure 9: Molecular interaction between ACOAT with Kaempferol-3-O-α-L-arabinopyranosyl (57401109)

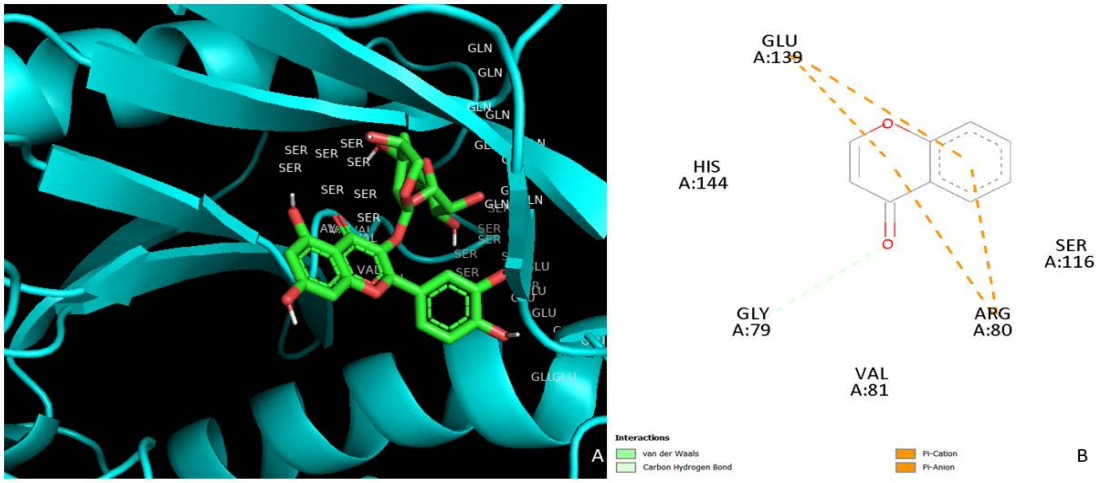

Figure 10: Molecular interaction between ACOAT with Quercetin-3-O-α-L-arabino pyranosyl (21722036)

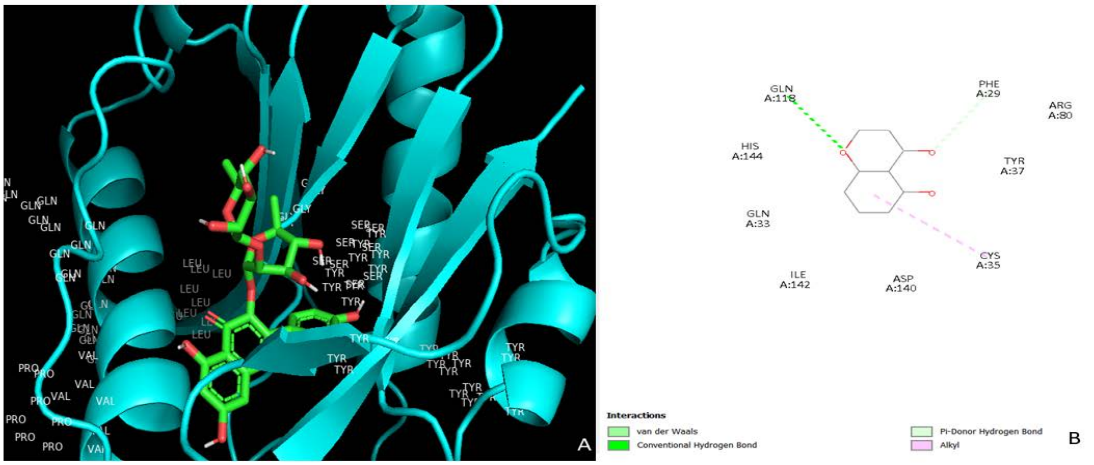

Figure 11: Molecular interaction between ACOAT with α-L-rhamno pyranoside (10698716)

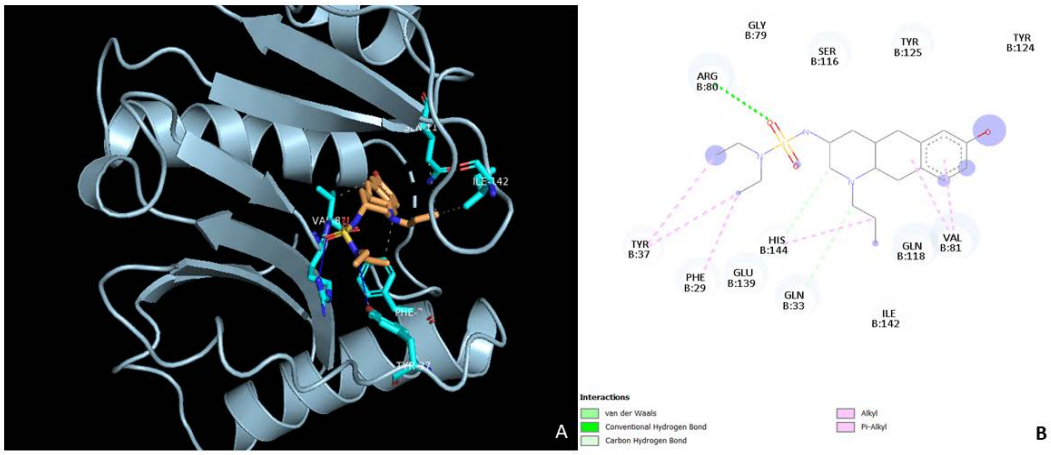

Figure 12: Molecular interaction between ACOAT with Sandoz (147031)

ADME analysis

ADME profiling of the selected phytochemicals was performed using the SwissADME tool. The phytochemicals of *Bryophyllum pinnatum* were evaluated for drug-likeness and pharmacokinetic properties using parameters such as Lipinski's Rule of Five, Lipophilicity (LogP), Topological Polar Surface Area (TPSA), Gastrointestinal Absorption (GIA), and Cytochrome P450 (CYP) inhibition. Among the analyzed compounds, CID 10742 showed the most favourable profile with no Lipinski violations, moderate LogP (1.54), acceptable TPSA (75.99 Å²), and high GIA, indicating good oral bioavailability, whereas several other phytochemicals with higher molecular weight and TPSA values exhibited low absorption and poor permeability. Most phytochemicals were predicted to be non-inhibitors of CYP enzymes and non-permeable to the blood-brain barrier, suggesting a safer metabolic and distribution profile. In contrast, the last compound representing the Sandoz-58-035 drug displayed balanced physicochemical properties with zero Lipinski violations, higher lipophilicity (LogP 3.19), acceptable TPSA (81.26 Å²), and high GIA similar to the best-performing phytochemical, but it showed CYP2C9 inhibitory activity, indicating a potential risk of drug-drug interactions. Overall, while many phytochemicals exhibit limited pharmacokinetic efficiency, selected compounds such as CID 10742 demonstrate comparable drug-like characteristics to the Sandoz-58-035 drug with a relatively improved safety profile due to the absence of CYP inhibition, making them promising candidates for further investigation. We compare the pharmacokinetic advantages. So the ADME analysis conducted in this study confirmed that the top-performing phytochemicals satisfied the Lipinski rule of five, suggesting favourable oral bioavailability and high gastrointestinal absorption. Notably, epigallocatechin-3-o-syringate and quercetin derivatives demonstrated higher predicted bioavailability, minimal CYP450 enzyme interactions, and lower toxicity profiles compared to traditional synthetic treatments. Similar analyses from prior studies have identified the limitations of statins due to their interactions with CYP3A4 and CYP2C9, which can complicate clinical outcomes and necessitate ongoing monitoring. In contrast, the results of this investigation point to naturally derived compounds with a lower risk of such interactions, making them more suitable candidates for long term therapeutic use. After that we compare the result of molecular dynamics simulation with Gyebi et al., they have utilized molecular dynamics simulations to assess the stability of enzyme-phytochemical interactions for synthetic compounds, our results highlight a marked improvement in the binding stability of selected phytochemicals. The top six enzyme-phytochemical complexes in this study retained strong interactions across the MD simulation period, suggesting longer binding durations and improved enzymatic inhibition compared with synthetic controls. These findings imply that the selected natural compounds maintain their effectiveness in a dynamic biological environment and can potentially sustain therapeutic activity over an extended period. While conventional treatments have long served as the cornerstone for managing hyperlipidaemia, their adverse effects and interaction profiles have fuelled the search for safer alternatives. The results of this investigation underscore the therapeutic promise of naturally sourced compounds like epigallocatechin-3-o-syringate, quercetin derivatives, and kaempferol-based ligands. Not only do these compounds exhibit stronger binding affinities and higher specificity for target enzyme active sites, but their ADME profiles also point toward improved safety, making them ideal candidates for further experimental and clinical validations (Table 11).

Table 11: SwissADME results

Plant and drug	Compounds	Formula	MW (g/mol)	NHD	NHA	LogP (iLogP)	Lipinski's RO5	NRB	TPSA (A°2)	Veber's rule	logKp cm/s	GIA	BBB	P-gp sub strate	CYP1A2 inhibitor	CYP2C19 inhibitor	CYP2C9 inhibitor	CYP2D6 inhibitor	CYP3A4 inhibitor
Bryophyllum pinnate	10742	$C_9H_{10}O_5$	198.17	2	5	1.54	0	3	75.99	0	-6.77	High	No	No	No	No	No	No	No
	131752831	$C_9H_8O_3$	164.16	2	3	2.94	0	2	188.51	1	-8.05	Low	No	Yes	No	No	No	No	Yes
	5488539	$C_{20}H_{18}O_{11}$	434.35	7	11	1.57	2	4	190.28	1	-8.25	Low	No	No	No	No	No	No	No
	57401109	$C_{26}H_{28}O_{14}$	564.49	8	14	2.24	3	5	228.97	1	-10.11	Low	No	Yes	No	No	No	No	No
	10698716	$C_{27}H_{30}O_{15}$	594.52	9	15	1.61	3	5	249.2	1	-10.09	Low	No	Yes	No	No	No	No	No
	21722036	$C_{26}H_{28}O_{15}$	580.49	9	15	1.72	3	5	249.2	1	-10.32	Low	No	Yes	No	No	No	No	No
	637542	$C_{21}H_{20}O_{11}$	448.38	7	11	0.95	2	4	57.53	0	-6.26	High	Yes	No	No	No	No	No	No
Sandoz-58-035	147031	$C_{20}H_{33}N_3O_3S$	395.56	6	2	3.19	0	7	81.26	0	-6.54	High	No	Yes	No	No	No	Yes	No

MD-simulation analysis

The top one enzyme-phytochemical complexes with the most favourable binding energies obtained from molecular docking were selected for Molecular Dynamics (MD) simulation to evaluate the stability and binding duration of the phytochemicals with their respective enzymes. Additionally, MD simulations were also performed for the enzyme in complex with the Sandoz-58-035 drug to enable a comparative evaluation of binding stability and interaction behaviour.

RMSF (Root Mean Square Fluctuation)

The RMSF profiles demonstrate a comparable overall fluctuation pattern across all three systems, indicating that the global fold of the protein remains largely conserved during the simulation. However, distinct variations in residue-level flexibility were observed, particularly in loop regions and terminal segments. The apoprotein (blue curve) exhibited moderate fluctuations throughout the sequence, with prominent peaks observed around residues ~30-40, ~80-90, and ~120-140, reaching values up to approximately 0.45-0.53 nm (Figure 13). These elevated fluctuations are characteristic of flexible loop regions and solvent-exposed domains, which typically exhibit higher mobility in the absence of phytochemical constraints. In comparison, the protein-phytochemical complex with the proposed compound (black curve) showed a noticeable reduction in fluctuations across several key regions, particularly within residues ~30-40 and ~80-100. The RMSF values in these regions were consistently lower than those of the apoprotein, indicating that phytochemical binding restricts local mobility and enhances structural rigidity. This stabilization effect suggests strong intermolecular interactions between the protein and the proposed ligand, which likely contribute to maintaining the integrity of the binding pocket. Notably, although minor fluctuations were observed toward the C-terminal region (~140-150 residues), these are commonly associated with terminal flexibility and are not indicative of global instability. Reduced RMSF values upon phytochemical binding are widely interpreted as evidence of stable protein-phytochemical interactions and decreased conformational entropy.

Conversely, the protein-drug complex with the Sandoz-58-035 phytochemical (red curve) displayed relatively higher fluctuations in several regions, particularly around residues ~80-100 and ~120-140. These fluctuations approached or exceeded those observed in the apoprotein, suggesting that the reference phytochemical does not effectively constrain residue mobility within these regions. The increased flexibility may reflect weaker binding interactions or suboptimal accommodation of the phytochemical within the active site, potentially leading to local structural perturbations. Such elevated RMSF values have been associated with reduced binding stability and dynamic instability in protein-phytochemical systems.

A comparative assessment clearly indicates that the proposed phytochemical (21722036) confers greater stabilization at the residue level than the reference Sandoz-58-035 ligand. The suppression of fluctuations in critical regions-particularly those likely associated with the active site or functional loops-suggests improved binding affinity and stronger intermolecular interactions. Additionally, the consistency between RMSD and RMSF findings reinforces the conclusion that the proposed phytochemical promotes both global and local structural stability.

The RMSF analysis highlights that phytochemical binding significantly influences residue-level dynamics, with the proposed compound demonstrating superior capability in stabilizing flexible regions of the protein. These findings support its potential as a more effective inhibitor and are consistent with contemporary molecular dynamics studies, where reduced residue fluctuations correlate with enhanced binding stability and functional inhibition (Figures 13 and 14).

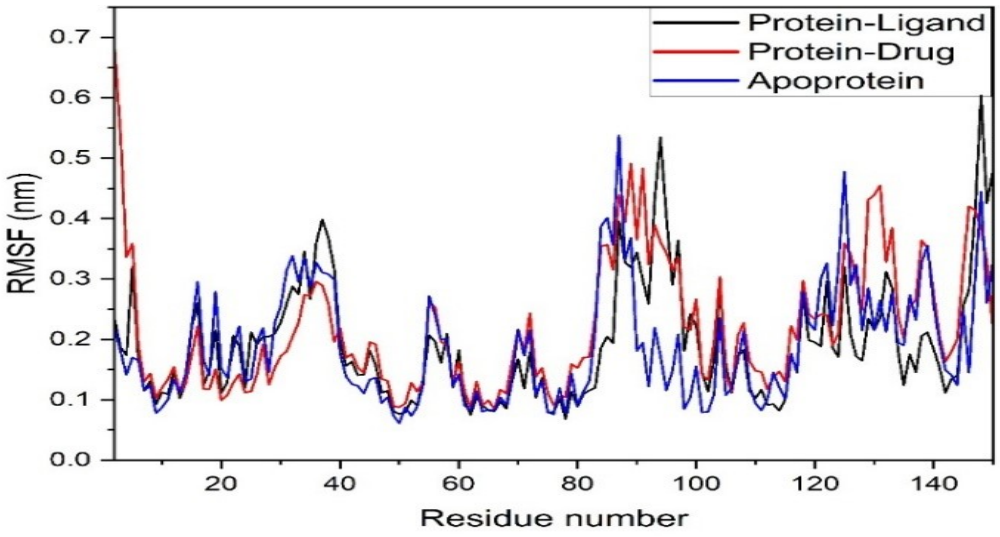

Figure 13: Root mean square fluctuation result

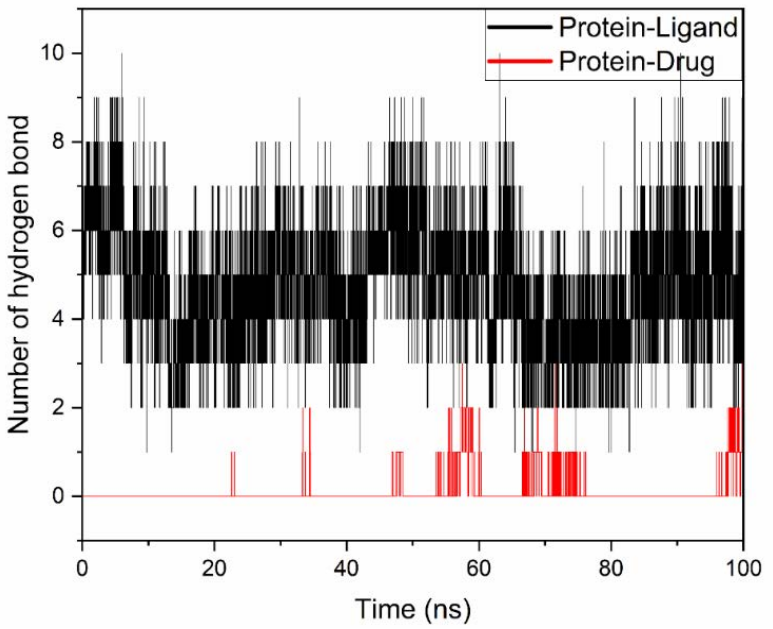

Figure 14: H-Bond analysis result.

H-bond analysis

The protein-phytochemical complex with the proposed compound (21722036) (black trace) exhibited a consistently higher number of hydrogen bonds throughout the simulation trajectory. The number of hydrogen bonds fluctuated predominantly between 4 and 8, with occasional peaks reaching up to 9-10 interactions, particularly during the initial (0-10 ns) and later stages (80-100 ns) of the simulation. Importantly, the system maintained a stable average of approximately 5-6 hydrogen bonds, indicating persistent and strong intermolecular interactions (Figure 14). The continuity and density of hydrogen bond formation across the entire simulation suggest that the proposed phytochemical remains stably anchored within the binding pocket, contributing to sustained structural integrity. Such persistent hydrogen bonding networks are widely associated with enhanced binding affinity and long-term stability in protein-phytochemical systems.

In contrast, the protein-drug complex with the Sandoz-58-035 phytochemical (red trace) displayed a markedly lower number of hydrogen bonds, with values frequently oscillating between 0 and 2 interactions throughout the simulation. Notably, extended periods with no hydrogen bond formation (0 bonds) were observed, particularly between ~10-50 ns and intermittently thereafter. Although occasional transient interactions (up to 2 hydrogen bonds) appeared during later stages (50-100 ns), these were not sustained, indicating weak and unstable binding. The intermittent nature of hydrogen bonding suggests that the Sandoz-58-035 phytochemical does not maintain consistent interactions within the active site, which may lead to reduced binding affinity and increased conformational flexibility. Such sporadic hydrogen bonding behaviour is often indicative of poor phytochemical accommodation and lower complex stability.

Comparative analysis clearly demonstrates that the proposed phytochemical (21722036) forms a significantly more stable and persistent hydrogen bonding network with the protein compared to the reference ligand. This observation aligns well with the RMSD and RMSF results, where the proposed phytochemical also exhibited enhanced structural stability and reduced residue fluctuations. The strong correlation between sustained hydrogen bonding and reduced conformational deviations reinforces the conclusion that the proposed compound promotes a more stable binding mode.

Furthermore, the presence of multiple hydrogen bonds throughout the simulation suggests that the proposed phytochemical likely engages key active-site residues, potentially enhancing specificity and inhibitory efficiency. In molecular dynamics studies, a higher number and persistence of hydrogen bonds are often directly correlated with stronger binding free energy and improved pharmacological potential.

The hydrogen bond analysis provides compelling evidence that the proposed phytochemical exhibits superior binding stability and interaction persistence compared to the Sandoz-58-035 ligand. These findings strongly support its potential as a more effective inhibitor of *Bacillus anthracis* acetyl-CoA acetyltransferase and validate its candidacy for further computational and experimental investigation.

SASA (Solvent Accessible Surface Area)

The apoprotein (blue curve) exhibited moderate fluctuations in SASA values throughout the simulation, ranging approximately between 88 and 98 nm². An initial decrease in SASA was observed during the early simulation

phase (~0-15 ns), followed by gradual stabilization with slight fluctuations around ~92-96 nm² (Figure 15). This behaviour suggests minor structural rearrangements leading to a relatively stable and equilibrated conformation. The observed fluctuations are typical for proteins in their unbound state, where solvent-exposed regions, particularly flexible loops, contribute to variability in surface area.

The protein-phytochemical complex with the proposed compound (21722036) (black curve) demonstrated comparatively stable SASA behavior, generally fluctuating within the range of 90-100 nm². Notably, the system showed a relatively higher SASA during the initial phase (~0-30 ns), followed by a slight reduction and stabilization toward the later stages of the simulation. This pattern indicates that the protein undergoes initial conformational adjustments upon phytochemical binding, followed by the adoption of a more compact and stable structure. The moderate SASA values suggest an optimal balance between structural compactness and necessary flexibility, which is often associated with stable and functionally relevant protein-phytochemical interactions.

In contrast, the protein-drug complex with the Sandoz-58-035 phytochemical (red curve) displayed a distinct decrease in SASA values, particularly between ~30-60 ns, where the surface area dropped to approximately 84-90 nm², followed by partial recovery in the later stages. This pronounced reduction in SASA may indicate excessive structural compaction or partial collapse of solvent-exposed regions, which can be associated with conformational instability or suboptimal phytochemical accommodation. The increased fluctuations observed across the trajectory further suggest that the system does not achieve a consistent equilibrium state. Such irregular SASA behavior is often indicative of unstable binding interactions and conformational strain within the protein structure.

Comparatively, the proposed phytochemical (21722036) maintains a more consistent SASA profile than the reference Sandoz-58-035 ligand, indicating a more stable structural arrangement with balanced solvent exposure. While the apoprotein exhibits expected baseline fluctuations, phytochemical binding-particularly with the proposed compound-appears to regulate solvent accessibility without inducing excessive compaction or instability. This observation aligns with the RMSD, RMSF, and hydrogen bond analyses, all of which consistently suggest enhanced stability of the protein in the presence of the proposed ligand.

The SASA analysis demonstrates that the proposed phytochemical promotes a stable and well-balanced conformational state, whereas the reference phytochemical induces irregular compaction and increased structural fluctuations. These findings reinforce the hypothesis that phytochemical 21722036 exhibits superior binding characteristics and contributes to maintaining the structural integrity of *Bacillus anthracis* acetyl-CoA acetyltransferase. The results are consistent with contemporary molecular dynamics studies, where stable SASA profiles correlate with favourable protein-phytochemical interactions and thermodynamic stability (Figures 15 and 16).

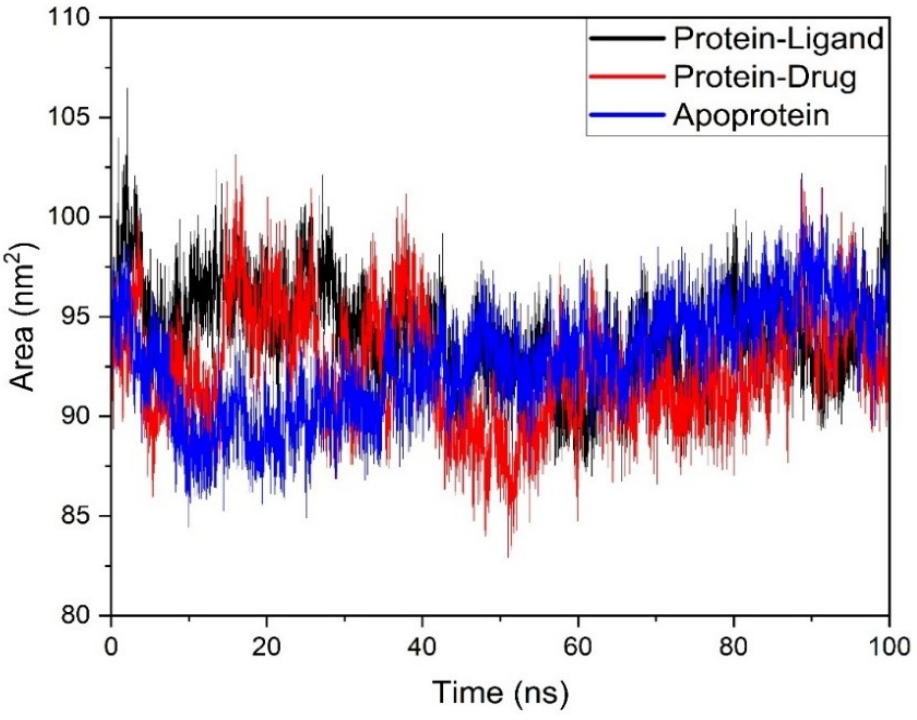

Figure 15: Solvent accessible surface area

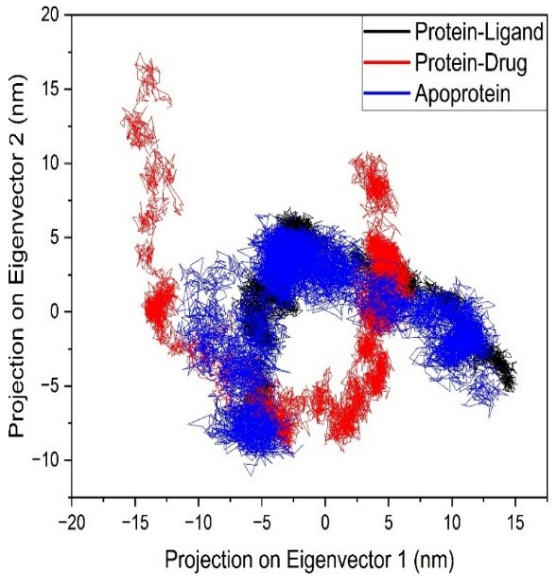

Figure 16: Principal component analysis

PCA (Principal Component Analysis)

The apoprotein (blue cluster) exhibits a relatively broad conformational distribution across the PCA space, spanning approximately from -15 to +12 nm along PC1 and -10 to +6 nm along PC2. This wide dispersion indicates that, in the absence of phytochemical binding, the protein explores a larger conformational space, reflecting higher intrinsic flexibility and dynamic freedom. Such extensive conformational sampling is characteristic of unbound proteins, where the absence of stabilizing interactions allows access to multiple conformational substates.

The protein-drug complex with the Sandoz-58-035 phytochemical (red cluster) displays an even more pronounced dispersion, particularly along PC2, where projections extend up to ~+17 nm. Additionally, the distribution appears fragmented into multiple distinct clusters rather than a single cohesive basin. This scattered and discontinuous conformational space suggests the presence of multiple metastable states and frequent transitions between them, indicative of conformational instability and reduced dynamic coherence. The broad and discontinuous sampling implies that the reference phytochemical fails to effectively stabilize the protein structure, leading to increased structural heterogeneity. Such behaviour is often associated with weak binding affinity and suboptimal phytochemical accommodation within the active site.

In contrast, the protein-phytochemical complex with the proposed compound (21722036) (black cluster) demonstrates a significantly more compact and well-defined conformational space, primarily localized within a narrower region of the PCA plot. The clustering is more continuous and less dispersed compared to both the apoprotein and the reference phytochemical system. This restricted conformational sampling indicates that the proposed phytochemical effectively limits large-scale motions and stabilizes the protein in a preferred conformational state. The presence of a dense and localized cluster is indicative of a dominant energy minimum and reduced conformational entropy, which are hallmarks of stable protein-phytochemical complexes.

Comparative analysis of the three systems clearly reveals that the proposed phytochemical induces greater conformational confinement and dynamic stability than the Sandoz-58-035 ligand. While the apoprotein exhibits natural flexibility and the reference phytochemical introduces excessive conformational heterogeneity, the proposed compound promotes a balanced dynamic profile characterized by reduced structural fluctuations and coherent motion. This observation is in strong agreement with the RMSD, RMSF, hydrogen bonding, and SASA analyses, all of which consistently indicate enhanced stability in the presence of phytochemical 21722036.

Furthermore, the compact clustering observed for the proposed phytochemical suggests the formation of a stable free energy basin, which is likely to correspond to a favorable binding mode. In molecular dynamics studies, such confined conformational spaces are directly associated with energetically favourable states and improved binding efficiency.

The PCA results provide compelling evidence that the proposed phytochemical (21722036) significantly enhances conformational stability and restricts unnecessary protein motions, thereby supporting its potential as a more effective inhibitor of *Bacillus anthracis* acetyl-CoA acetyltransferase. The ability of the phytochemical alto reduce conformational entropy while maintaining structural integrity further strengthens its candidacy for drug development.

FEL (Free Energy Landscape analysis)

The apoprotein system (Figure 17) exhibits a moderately

broad free energy landscape characterized by multiple shallow minima distributed across the conformational space. The presence of several low-energy basins connected by relatively smooth transitions suggests that the unbound protein samples a range of conformations with comparable stability. This behaviour reflects the inherent flexibility of the protein in the absence of phytochemical constraints, allowing transitions between metastable states. Such multi-basin landscapes are typical for apo systems, where conformational plasticity is essential for functional adaptability.

In contrast, the protein-drug complex with the Sandoz-58-035 phytochemical displays a more dispersed and fragmented free energy landscape. Multiple distinct minima are observed, separated by higher energy barriers, indicating the presence of several competing conformational states. The distribution appears less continuous and more scattered compared to the apoprotein, suggesting reduced conformational coherence and increased energetic heterogeneity. This fragmentation implies that the system undergoes frequent transitions between unstable or semi-stable states, reflecting weaker binding interactions and an inability of the phytochemical to stabilize a dominant conformational basin. Such landscapes are often associated with reduced binding affinity and dynamic instability in protein-phytochemical systems.

Conversely, the protein-phytochemical complex with the proposed compound (21722036) demonstrates a markedly different behaviour, characterized by a well-defined and deep global minimum with a more confined and continuous energy basin. The FEL reveals a dominant low-energy region with fewer scattered minima, indicating that the system predominantly occupies a single, energetically favourable conformational state. The depth of the basin (lower Gibbs free energy) and the reduced spread across PC1 and PC2 suggest enhanced thermodynamic stability and restricted conformational sampling. This indicates that the proposed phytochemical effectively stabilizes the protein structure, minimizing unnecessary conformational transitions and promoting a coherent dynamic profile.

Comparative analysis across the three systems clearly highlights that the proposed phytochemical induces a more stable and energetically favourable conformational landscape than both the apoprotein and the reference Sandoz-58-035 ligand. While the apoprotein retains natural flexibility and the reference phytochemical introduces energetic fragmentation, the proposed compound promotes a single dominant energy basin, which is a hallmark of strong and stable protein-phytochemical interactions. This observation is in excellent agreement with the PCA results, where the proposed phytochemical also exhibited compact clustering, as well as with RMSD, RMSF, SASA, and hydrogen bond analyses, all consistently indicating enhanced structural stability.

Furthermore, the formation of a deep and well-defined energy minimum suggests that the proposed phytochemical reduces conformational entropy while stabilizing the protein in its most favorable binding conformation. In molecular dynamics studies, such FEL characteristics are directly correlated with improved binding affinity, higher residence time, and enhanced inhibitory potential.

The FEL analysis provides compelling thermodynamic evidence that the proposed phytochemical (21722036) exhibits superior binding stability and conformational control compared to the reference Sandoz-58-035 ligand. The ability to confine the protein within a stable low-energy basin strongly supports its potential as an effective inhibitor of *Bacillus anthracis* acetyl CoA acetyltransferase and reinforces the conclusions drawn from other dynamic and structural analyses.

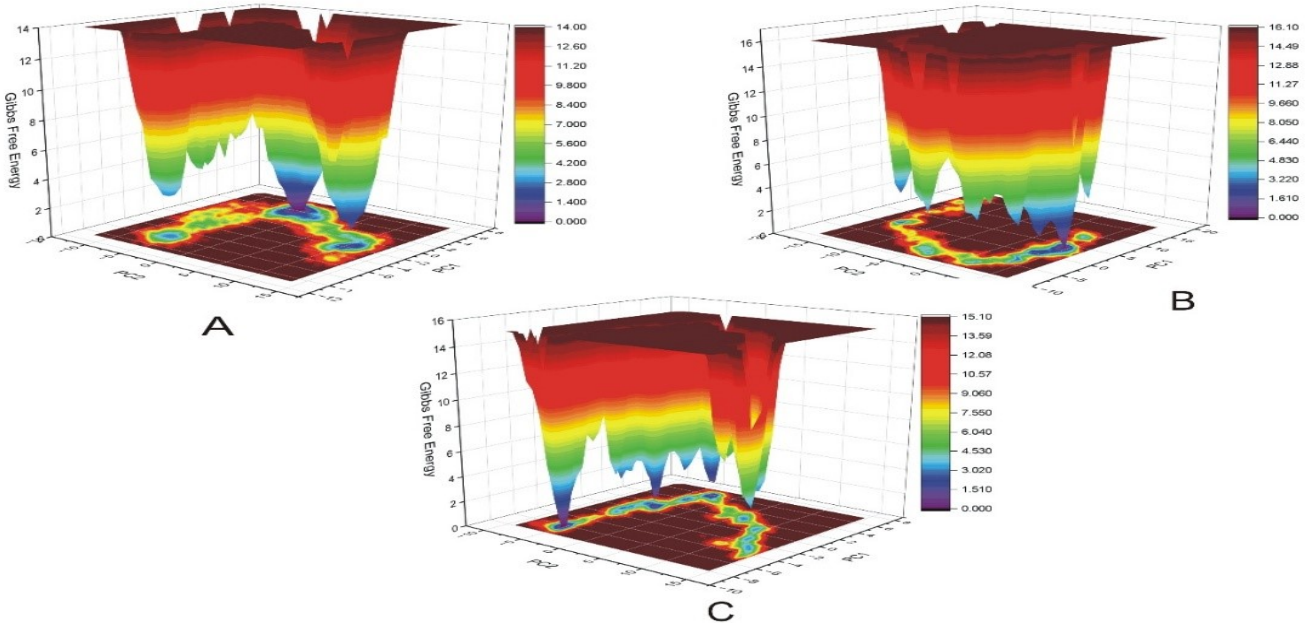

Figure 17: Free energy landscape analysis

Conclusion

The present study highlights the potential of plant-derived phytochemicals as effective inhibitors of acetyl-CoA acyltransferase, a key enzyme involved in lipid metabolism. Through an integrated computational approach, including molecular docking, ADME profiling, and molecular dynamics simulation, several phytochemicals demonstrated strong binding affinity, favourable pharmacokinetic properties, and stable interactions with the target enzyme. Notably, some compounds exhibited better performance compared to the standard drug, indicating their promising therapeutic potential. These findings suggest that natural phytochemicals may serve as safer alternatives for the long-term management of lipid metabolism disorders, with reduced risk of adverse effects commonly associated with synthetic drugs. However, despite encouraging *in silico* results, further experimental validation through *in vitro* and *in vivo* studies is essential to confirm their efficacy, safety, and clinical applicability. Overall, this study provides a valuable foundation for the development of novel plant-based therapeutic strategies targeting lipid-related disorders.

References

1. D. J. Murphy, The biogenesis and functions of lipid bodies in animals, plants and microorganisms, Prog Lipid Res, 40(2001):325-438.
2. Q. Q. Tang, Lipid metabolism and diseases, Sci Bull, 61(2016):1471-1472.
3. M. Y. Cui, X. Yi, D. X. Zhu, J. Wu, Aberrant lipid metabolism reprogramming and immune microenvironment for gastric cancer: A literature review, Transl Cancer Res, 10(2021):3829.
4. M. G. Saklayen, The global epidemic of the metabolic syndrome, Curr Hypertens Rep, 20(2018):1-8.
5. M. Ruscica, N. Ferri, M. Banach, C. R. Sirtori, A. Corsini. Side effects of statins: From pathophysiology and epidemiology to diagnostic and therapeutic implications, Cardiovasc Res, 118(2022):3288-3304.
6. V. Balamurugan, S. Fatima, S. Velurajan, A guide to phytochemical analysis, Int J Adv Res Innov Ideas Educ, 5(2019):236-245.
7. K. Kumar, A. K. Malaisamy, R. Sharma, K. Ranjan, R. Satpathy, et al. *In silico* approach to screen anti-inflammatory phytochemicals: Targeting cytosolic phospholipase A2 and phospholipase C, J Biomol Struct Dyn, 1(2025):1-10.
8. R. Kumar, Honey in food science and physiology, Honey Food Sci Physiol, (2024):121.
9. R. Lal Swagat Shrestha, B. P. Marasini, J. Adhikari Subin, Phytochemicals of *Swertia chirayita* Roxb. ex Fleming against malarial dihydroorotate dehydrogenase: An *in silico* study, Discov Molecules, 1(2024):3.
10. B. Larbaoui, R. Menad, Single-click molecular docking *via* SwiftDock: A new virtual screening tool using AutoDock4, Comput Struct Biotechnol Rep, 1(2024):100017.
11. A. Pawar, H. Deka, M. Battula, H. M. Aljawdah, P. C. Patil, et al. Integrated machine learning and physics-based methods assisted *de novo* design of Fatty Acyl-CoA synthase inhibitors, Expert Opin Drug Discov, 20(2025):123-135.
12. G. T. Galdino, T. DesCôteaux, N. Teruel, R. Najmanovich, NRGSuite-Qt: A PyMOL plugin for high-throughput virtual screening, molecular docking, normal-mode analysis, the study of molecular interactions and the detection of binding-site similarities, Bioinform Adv, (2025):vbaf129.
13. M. J. Yousef, N. F. Oliveira, J. N. Vitorino, P. B. Reis, P. Draczkowski, et al. Toward accurate pH-dependent binding constant predictions using molecular docking and constant-pH MD calculations, J Chem Theory Comput, 21(2025):2655-2667.
14. A. Das, S. Burman, C. Das, M. Bhadra, S. Mondal, et al. An insight into the bactericidal and phytochemical properties of leaf extract of *Vernonia squarrosa* and understanding antibacterial activity by molecular docking, Pharmacol Res Mod Chin Med, 12(2024):100502.
15. M. Yadav, D. Yadav, D. P. Singh, J. K. Kapoor, Macrocyclic Schiff base complexes of Zn (II), Cu (II), Co (II), and Ni (II) targeting topoisomerase IIβ: Synthesis, docking, and evaluation as potential anticancer agents, Appl Organomet Chem, 39(2025):e7885.
16. SwissADME tool, SwissADME, (2026).
17. M. Azmal, M. S. Hossen, M. N. H. Shohan, R. Taqui, A. Malik, et al. A computational approach to identify phytochemicals as potential inhibitor of acetylcholinesterase: Molecular docking, ADME profiling and molecular dynamics simulations, PLoS One, 19(2024):e0304490.
18. S. S. Swain, T. Hussain, Combined bioinformatics and combinatorial chemistry tools to locate drug-able anti-TB phytochemicals: A cost-effective platform for natural product-based drug discovery, Chem Biodivers, 19(2022):e202200267.
19. S. Cho, H. Jo, Y. J. Hwang, C. Kim, Y. H. Jo, et al. Potential impact of underlying diseases influencing ADME in nonclinical safety assessment, Food Chem Toxicol, (2024):114636.
20. A. C. Beatrice, Advancements and future directions in molecular dynamics (MD) simulations, IDOSR J Appl Sci, 9(2024):21-26.